Bollettino di Geofisica Teorica ed Applicata Vol. 61, n. 1, pp. 41-56; March 2020
DOI 10.4430/bgta0251

PS-InSAR data analysis: pre-seismic ground deformation in the 2009 L'Aquila earthquake region

S. Nardò[1], A. Ascione[1], S. Mazzoli[1], C. Terranova[2] and G. Vilardo[3]

[1] *Department of Earth, Environmental and Resources Sciences, University 'Federico II', Naples, Italy*
[2] *AT Sogesid/MATTM "Geoportale Nazionale\Telerilevamento", Rome, Italy*
[3] *Istituto Nazionale di Geofisica e Vulcanologia, Osservatorio Vesuviano, Naples, Italy*

(Received: 1 April 2018; accepted: 1 October 2018)

ABSTRACT The accuracy of the millimetre-scale measurements made so far by the SAR systems, as well as the multi-temporal analysis methodologies, have provided impressive images of surface displacements in areas affected by strong earthquakes, and contributed to constrain the geometric and kinematic features of earthquake generating faults. The multi-temporal analysis of InSAR data is also being acknowledged as promising for the search of earthquake precursors. We have applied the multi-temporal PS-InSAR technique to the detection of pre- to post-seismic ground displacements in the region struck by the normal faulting 2009 L'Aquila earthquake. We have used ERS and ENVISAT PS-data sets from both ascending and descending orbits, covering a 20-year long time span. On the yearly-scale, we have identified a pre-seismic displacement pattern, which consists of opposite vertical motions that have affected the blocks in the hanging wall and footwall of the structure that is recognised as the surface trace of the earthquake-generating fault. In particular, we have highlighted a pre-seismic uplift for 4-5 years followed by subsidence (starting 6-8 months prior to the earthquake) of the hanging wall block, coeval to opposite vertical motions of the footwall block. We suggest that such a displacement pattern may represent an earthquake precursor signal.

Key words: PS-InSAR, M_W 6.3 L'Aquila earthquake, ground deformation, pre-seismic, earthquake precursor, central Apennines.

1. Introduction

Remote sensing data by SAR interferometry (InSAR) provide a one-dimensional measurement of change in distance along the direction of the radar spacecraft (Line of Sight, LoS) for two orbit geometries, ascending and descending, whose combination results are two - vertical and horizontal - displacement vectors in an E-W oriented vertical plane. The technique is widely used to detect and monitor ground deformations induced by landslides, volcanism, tectonics and anthropic processes in urbanised areas (Massonnet and Rabaute, 1993; Achache *et al*., 1995; Carnec *et al*., 1996; Fruneau *et al*., 1996; Kimura and Yamaguchi, 2000; Berardino *et al*., 2002; Corsini *et al*., 2006; Tizzani *et al*., 2007; Vilardo *et al*., 2009).

The development of new techniques, such as the Permanent Scatterers technique and Small Baseline Subset (SBAS; Berardino *et al*., 2002), based on the analysis of large data sets and, more in general, the Differential SAR Interferometry approach (DInSAR), has significantly increased the potential of SAR remote sensing for ground deformation detection. The SAR technique has proved a powerful tool for exploring the slow motion of the Earth's surface at local (Ferretti *et al*., 2000; Prati *et al*., 2010) and sub-regional scale (Bürgmann *et al*., 2006; Corsini *et al*., 2006; Meisina *et al*., 2006). The SAR technique has also provided fundamental constraints on modelling earthquake source mechanisms (e.g. Stramondo *et al*., 1999; Atzori *et al*., 2009; D'Agostino *et al*., 2012; Cheloni *et al*., 2017). Such a technique is also well-suited for the detection of ground deformation possibly predating seismic events, a task crucial to forecasting strategies based on the search for diagnostic precursor signals of severe earthquakes (Jordan *et al*., 2011). In recent years, research has pushed forward towards the identification of pre-seismic ground deformation patterns through the use of SAR-based techniques, which are being acknowledged among the most promising tools for the search of earthquake precursors (Moro *et al*., 2017). Within such a framework, the interferometric Extraordinary Environmental Remote Sensing Plan (PST-A) archive, by the Italian Ministry of the Environment (MATTM), holds the millimetre ground deformation data that could be the most important marker of accumulation of crustal seismogenic stress. Such a data set may provide fundamental information on the pre-seismic phase of moderate to strong earthquakes that have struck Italy in recent years.

Our study focuses on pre-seismic ground deformation in the region struck by the M_W 6.3, 2009 L'Aquila earthquake. The 2009 L'Aquila earthquake was characterised by a normal faulting mechanism (Chiarabba *et al*., 2009; Cirella *et al*., 2009; Boncio *et al*., 2010; Chiaraluce *et al*., 2011). Coseismic deformation was identified by different geodetic and remote sensing (SAR) methods (Atzori *et al*., 2009; Cirella *et al*., 2009; Walters *et al*., 2009; Costantini *et al*., 2017), which allowed constraining the 6 April 2009 main shock source properties. However, only negligible pre-event displacement has been detected to date on longer time windows through both SAR data analysis and other geodetic methods (Amoruso and Crescentini, 2010; Lanari *et al*., 2010).

In this work, we use the products of Permanent Scatterers Synthetic Aperture Radar Interferometry (PS-InSAR) processing technique (Ferretti *et al*., 2000, 2001) to investigate the ground deformation in the 2009 L'Aquila earthquake region. In particular, with the aim of outlining a comprehensive framework of the pre-seismic behaviour of the L'Aquila region, we have investigated, through the multi-temporal PSInSAR technique, a roughly 20-year long period spanning over the M_W 6.3, 6 April 2009 L'Aquila main shock.

2. Seismotectonic and SAR remote sensing background of the 2009 L'Aquila earthquake

The 6 April 2009 L'Aquila earthquake struck causing heavy damage in the Aterno River (Fig. 1) middle valley Quaternary basin in central Italy (Galli *et al*., 2009; Santo *et al*., 2014, and references therein).

The M_W 6.3, 6 April 2009 mainshock was preceded by foreshocks that started in October 2008 (Di Luccio *et al*., 2010). In the following months, many aftershocks were recorded including

two strong aftershocks with M_W 5.4 and M_W 5.6 (Di Luccio *et al*., 2010; Papadopoulos *et al*., 2010; Valoroso *et al*., 2013). The main shock hypocentre was located at about 9 km depth along a NW-SE striking normal fault, dipping at 55°-60° (Chiarabba *et al*., 2009; Pondrelli *et al*., 2010; Scognamiglio *et al*., 2010). The surface expression of the structure activated by the 2009 earthquake has been associated with the Paganica - San Demetrio fault system [PSDFS, *sensu* Galli *et al*. (2010), Fig. 1], a 18-20 km long, NW-SE trending fault system composed of several, few kilometres long segments with dextral *en-echelon* arrangement and dipping to the SW (Galli *et al*., 2010, 2011). The earthquake caused several ground ruptures (open cracks and fractures with vertical offsets) mainly NW-SE trending and aligned along the PSDFS, but also affecting the Aterno River plain (Boncio *et al*., 2010; EMERGEO Working Group, 2010), some of which have been interpreted as surface faulting (Falcucci *et al*., 2009; Lavecchia *et al*., 2009). Vertical offsets of superficial fractures were mostly within 10 cm (Galli *et al*., 2010).

Besides the seismological and field data, a huge amount of information fundamental to the reconstruction of the 2009 L'Aquila earthquake displacement field, and to constrain the earthquake source mechanism, has been obtained by analysing different types of remote sensing and geodetic data sets. GPS and DInSAR modelling of the co-seismic displacement field (Anzidei *et al*., 2009; Atzori *et al*., 2009; Walters *et al*., 2009; Papanikolaou *et al*., 2010) have concurred to define a 50° SW-dipping normal fault plane, geometrically consistent with both the mainshock seismogenic source and the southern segment of the PSDFS. In particular, the differential SAR interferograms have shown the deformation pattern generated by the fault slip, with a large sinking (~ -25 cm) of the downthrown block vs. ~ +5 cm in the raised block (Atzori *et al*., 2009; Walters *et al*., 2009; Papanikolaou *et al*., 2010). Similar values of the co-seismic deformation were estimated by GPS inversion (Cheloni *et al*., 2010).

SAR data analysis has also allowed detecting, in the region hit by the 2009 L'Aquila earthquake, post-seismic deformation [hanging wall subsidence: Lanari *et al*. (2010), D'Agostino *et al*. (2012), Cheloni *et al*. (2014)], while less clear is the reconstruction of the pre-seismic deformation scenario. Lanari *et al*. (2010) by analysis of DInSAR time series (February 2003 to October 2009) from ENVISAT ascending track data sets in the 2009 epicentral area, point out that pre-seismic surface deformation is negligible. On the other hand, by applying DInSAR processing to ALOS and ENVISAT satellites data, Atzori *et al*. (2013) identify a far-field pre-seismic (from 2005) deformation process in the region to the west of the mainshock epicentre. Furthermore, by analysis of multiple SAR data sets (RADARSAT, ENVISAT and COSMO-SkyMed), Moro *et al*. (2017) recognise in two sub-basins of the middle Aterno valley basin located to the north of the mainshock (Pizzoli and Petruro basins; Fig. 1), up to 15 mm of subsidence in the three years before the main shock and post-seismic uplift up to 12 mm. In both cases, a relationship with seismically-induced fluctuations of the groundwater table has been hypothesised.

3. Materials and method

With the InSAR technique, deformations are detected as phase variations of the electromagnetic signal, through a multitemporal acquisition of SAR images, along the satellite LoS; (Fig. 2). From the methodological point of view, differential interferometry is applied in terms of stacking of

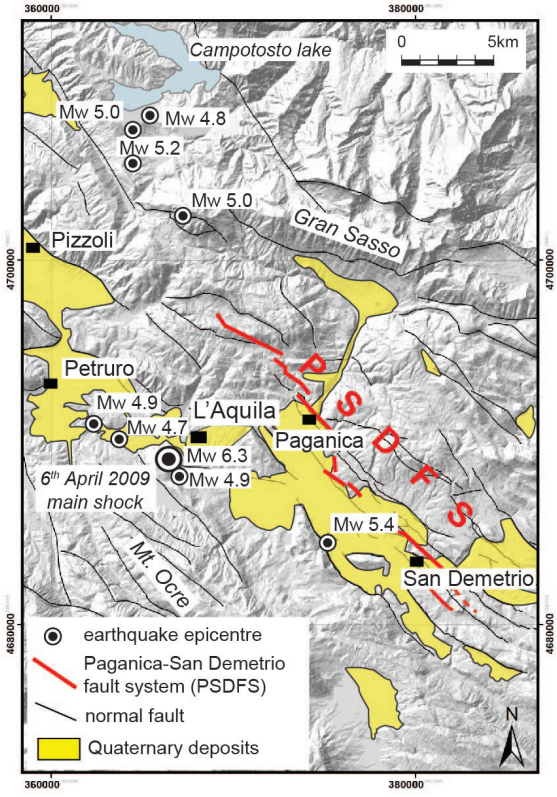

Fig. 1 - The 2009 L'Aquila earthquake epicentre region, with location of PSDFS, (*sensu* Galli *et al.*, 2010). Locations of epicentres of the M_w 6.3, 6 April 2009 main shock and of the strongest aftershocks (from the ISIDe catalogue: http://cnt.rm.ingv.it/iside), are also shown. The central sector of the Aterno River valley is NW-SE trending and includes several sub-basins located from Pizzoli, to the north, to San Demetrio, to the south.

interferograms using SBAS [Small Baseline Subset: Berardino *et al.* (2002)] and/or PS (Permanent Scatterer) techniques. In our work, we have used the PS-InSAR technique (Ferretti *et al.*, 2000, 2001). PSs correspond to man-made objects (structures on the roofs of buildings, utility poles, dams, etc.) or natural (rock outcrops) reflectors characterised by stable individual electromagnetic radar phase signal over long temporal series of interferometric SAR images. The phase data from PS are used to detect topographic changes in time. The availability of about a 20-year long PS-InSAR data coverage of the Italian territory - MATTM data sets comprising the April 1992 to December 2000 time span for ERS satellites and the November 2002 to June 2010 time span for ENVISAT satellite data, acquired from both the ascending and descending orbits - has allowed us to perform the analysis of ground deformation of the investigated region during a time window that predates and postdates the 2009 L'Aquila earthquake. We have analysed both the ERS (1991 - 2000) and ENVISAT (2003 - 2010) PS data sets (Table 1). ERS and ENVISAT PS data from the MATTM database are high quality (coherence index ranging from 0.6 to 1.0). Specifically, for data in our study area the PS coherence index mean value is about 0.7, with standard deviations of PS mean velocity (in the 1991-2000 and 2003-2010 time spans) in the 0.4 to 0.5 mm/yr range, and of the deformation measurement error of ±3 mm, respectively.

In the analysed area, centred on the 2009 L'Aquila earthquake epicentre and 340 km^2 wide, there are 16,700 descending track ERS PSs (55 PS/km^2) and 12,000 ascending track ERS PSs (40 PS/km^2), and 29,000 ENVISAT descending track PSs (95 PS/km^2) and 39,000 ENVISAT ascending track PSs (130 PS/km^2), respectively. The PS spatial distribution is substantially homogeneous in the analysed area.

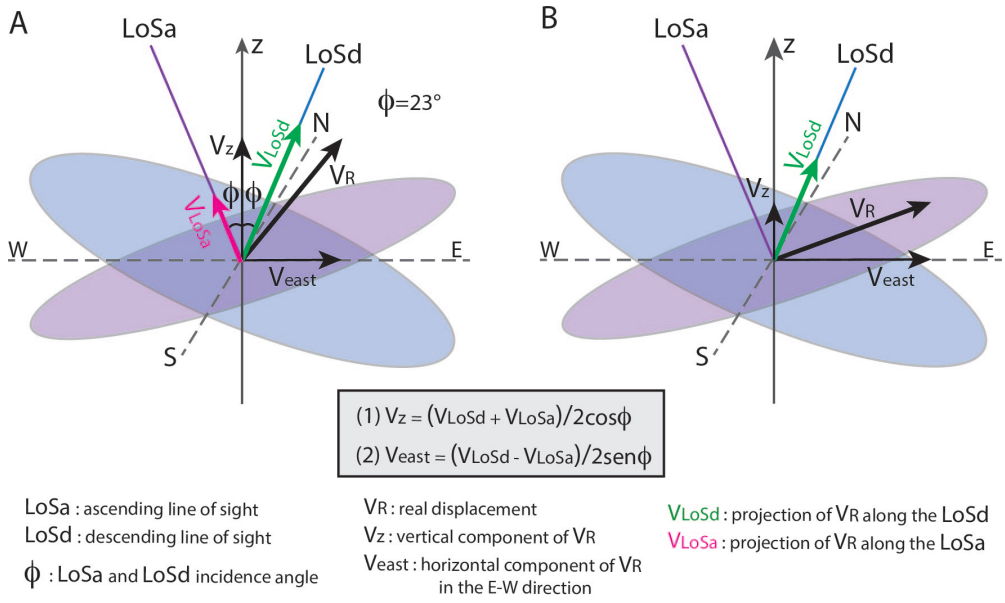

Fig. 2 - A: ERS and ENVISAT SAR geometry, showing LoS-oriented components of the real displacement vector (VR) along the descending and ascending satellite orbits, and in the up-down (z) and E-W planes; components of the real displacement vector (VR) oriented towards the north or south are not detected by the SAR. B: components of the real displacement vectors (VR) for PS motion occurring in a plane orthogonal to orientation of the ascending LoS, i.e. motion that is undetectable by SAR satellite in the ascending orbit, with an up-east orientation. Eqs. 1 and 2 are from: Lundgren *et al*. (2004), Manzo *et al*. (2006), Lanari *et al*. (2007), and Tofani *et al*. (2013).

Table 1 - PS data sets used in this work.

ERS	
DESCENDING TRACK	ASCENDING TRACK
pst_ers_t308_f2751_cl001_l_aquila (42573 PSs)	pst_ers_t129_f837_cl002_pineto (47650 PSs)
pst_ers_t308_f2769_cl001_sulmona (69065 PSs)	pst_ers_t129_f837_cl001_celano (126131 PSs)
ENVISAT	
DESCENDING TRACK	ASCENDING TRACK
PST2009_ENVISAT_T79_F2748_CL001_AQUILA (127089 PSs)	PST2009_ENVISAT_T401_F840_CL001_AQUILA (270047 PSs)
PST2009_ENVISAT_T308_F2751_CL001_TERAMO (341759 PSs)	PST2009_ENVISAT_T129_F837_CL001_CHIETI (308357 PSs)

A thorough inspection of all available individual ERS and ENVISAT PSs time series was performed with the aim of detecting temporal changes in the ground motion oriented along both the ascending and descending LoS. Based on the results of this inspection (section 4), the ENVISAT data set was selected for the further analyses described below.

Due to the SAR acquisition geometry, it is necessary to consider ascending - descending PSs pairs in order to compose the "real" displacement in the vertical plane (z) oriented W-E (Fig. 2A). Such a composition may be performed using a geometrical relationship (Lundgren *et al*., 2004; Manzo *et al*., 2006; Lanari *et al*., 2007; Tofani *et al*., 2013) linking the LoS displacement values and the LoS angle of incidence, which is $\Phi = 23°$ for both ERS and ENVISAT satellites

(Fig. 2). However, PS from ascending and descending images are neither spatially coincident nor exactly synchronous. In order to standardise the data sets from the temporal point of view, we have composed each image pair by selecting ascending-descending radar images with a time separation not larger than one month, ending with the composition of 24 radar image pairs for the 2005-2010 time span. Then, a GIS-aided spatial analysis was carried out to compile a set of raster interpolating maps of displacement values for the ascending and descending LoS, respectively. For the geospatial analysis, the Inverse Distance Weighting interpolator (IDW) statistics with 50×50 m^2 size cell was used. The ascending and descending LoS displacement maps were compiled for different time intervals of the pre- to post-seismic time span. Individual time intervals were set based on the results of the PS time series analysis (section 4.2).

The GIS-aided analysis was then applied to the compiling of maps of the vertical (z, up - down) component of the "real" displacement vector, following Eq. 1 of Fig. 2.

4. Results

4.1. ERS data set analysis

All available descending and ascending pairs of ERS PSs time series from the 2009 L'Aquila earthquake epicentral region were analysed. The descending LoS PS time series show a periodic, seasonal signal (Fig. 3A) within a general sub-horizontal trend. Such a trend indicates that mean PS velocities are around 0 mm/yr with respect to the descending LoS in the 1992-2000 time span (Fig. 3A). The ascending ERS PSs time series show irregular signals, although some seasonal oscillation is still identified (Fig. 3B). However, as for the descending orbit ERS PSs time series, the general trend is sub-horizontal with a resulting LoS-oriented mean velocity around 0 mm/yr.

Since trends of both the ascending and descending time series are sub-horizontal, the composition of the single pairs of PS according with SAR geometry (Fig. 2) does not show substantial vertical or horizontal (E-W oriented) ground deformation over the entire study region in the 1992-2000 time span.

4.2. ENVISAT data set analysis

An in-depth inspection of all of the available pairs of PSs ENVISAT time series from the study region has been carried out. As for the ERS time series, the ENVISAT time series show irregular and oscillating - seasonal - signals. Such signals are the main feature of the ascending time series in the 2004 to March 2009 time span (Fig. 4A). In other words, no clear displacement oriented towards, or opposite to, the LoS and an almost null mean velocity (sub- horizontal trend) with respect to the ascending LoS are observed throughout the pre-seismic period in the study region. The analysis also shows that PS time series from a wide area in the middle Aterno valley to the SW of the PSDFS, image a sudden downward motion during the co- to early post-seismic period (March 2009 - May 2009; e.g. Fig. 4A). The final part of the PS time series records (May 2009 - June 2010) show substantial absence of ground motion oriented along the ascending LoS (Fig. 4A).

More complex temporal evolution, and spatial distribution, of ground motions have been detected through the analysis of PS time series from the ENVISAT descending tracks. In particular, irregular and oscillating - seasonal - signals that characterise the PS time series appear as minor features of PS motion with respect to main trends oriented along the LoS. For instance, as is shown

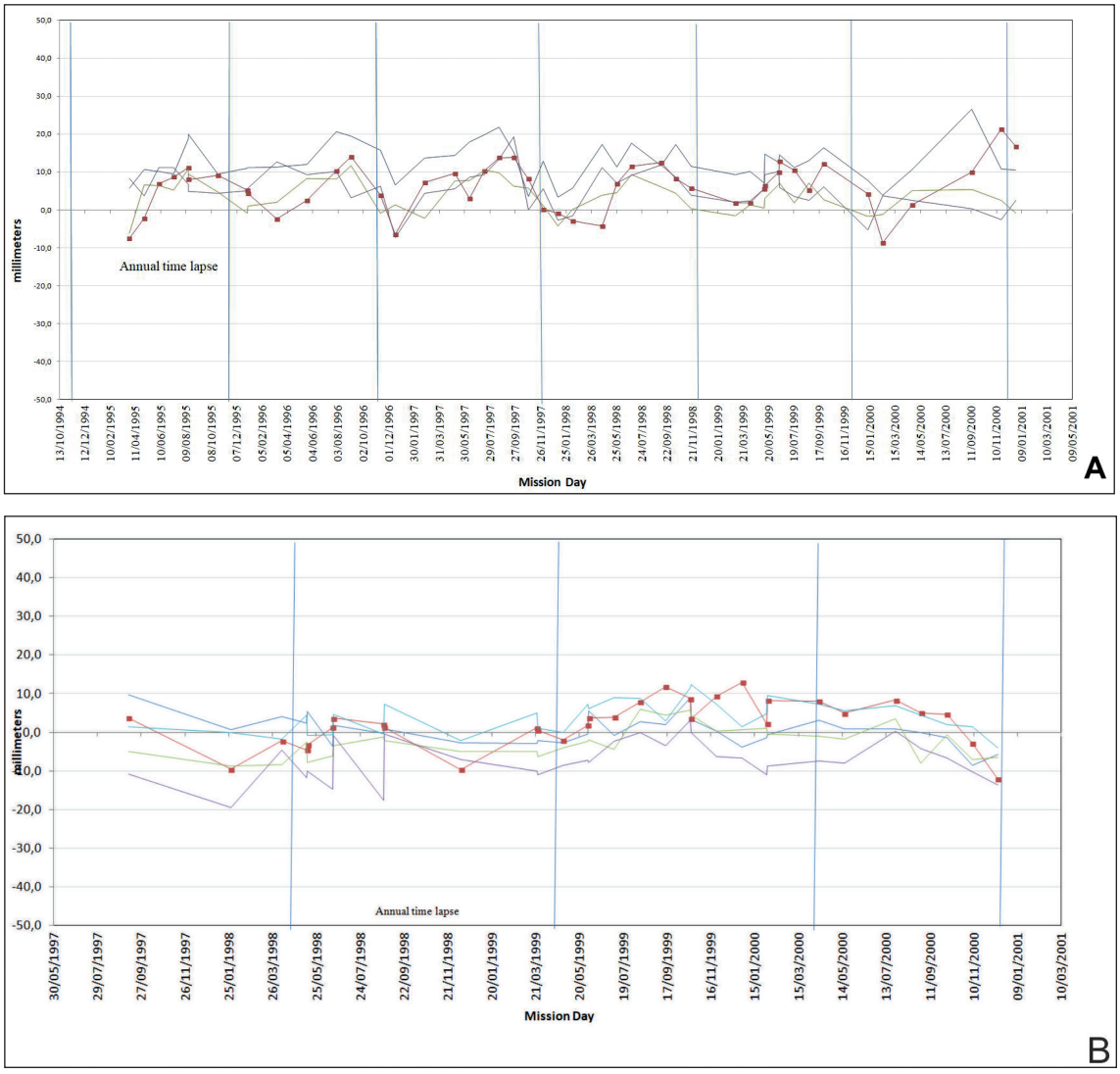

Fig. 3 - Examples of ERS (1992 - 2000) time series of PSs from the 2009 L'Aquila earthquake epicentral region (PSDFS fault hanging wall block). A: descending LoS time series: the general trend is sub-horizontal (mean velocity ~ 0 mm/yr), although the presence of a periodic and seasonal signal is evident. B: ascending LoS time series: the general trend is sub-horizontal, but the signal is quite noisy with a likely periodic, and seasonal, oscillation.

by the PS time series from an area close to the main shock epicentre, four main stages may be distinguished in the analysed time window (Fig. 4B). In a first time span (2004 to July - October 2008; Stage A in Fig. 4B), an upward motion oriented along the descending LoS is detected by the linear trend of the displacement. From July - October 2008 to the beginning of April 2009, the time series show a downward trend (Stage B in Fig. 4B). In the March - April 2009 to May - June 2009 time span, i.e. in the co-seismic to early post-seismic time span, a sudden downward motion is identified, followed by a subdued lowering from May/June 2009 to June 2010 (Stages C and D in Fig. 4B, respectively).

The different motion patterns that are detected by analysis of time series from the descending and ascending orbits find an explanation in the geometrical configurations of the two orbits (Fig.

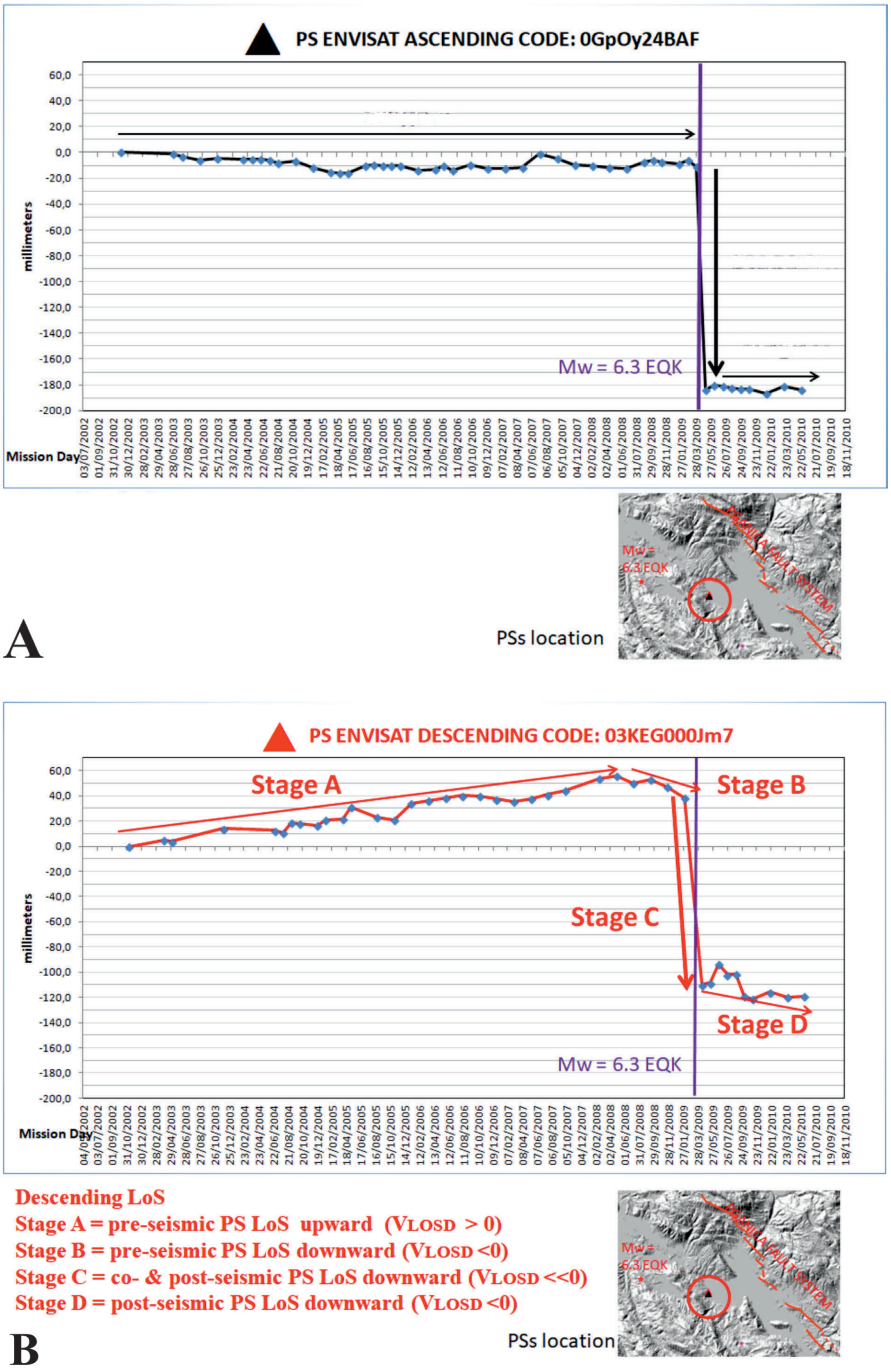

Fig. 4 - 2003 - 2010 time series of ENVISAT PSs pair from an area close to the 2009 L'Aquila earthquake epicentre (locations in inset maps). A: ascending LoS time series. Three stages may be distinguished: in a first stage (2004 - March 2009) the general trend is sub-horizontal (mean velocity ~ 0 mm/yr), meaning no net LoS upward or downward motion; in the short-time span that includes the 2009 L'Aquila main shock (March - May 2009) a sudden downward motion is identified; in the May 2009 - June 2010 time span the general trend is sub-horizontal. B: descending LoS time series. Four deformation stages may be distinguished in the 2004 - 2010 time span: Stage A (from 2004 to September/October 2008) corresponds to a positive (oriented upward towards the LoS) trend; Stage B (September/October 2008 - January/February 2009) corresponds to LoS downward trend; Stage C (March - May 2009) corresponds to a sudden LoS downward trend; Stage D (May 2009 - June 2010) corresponds to a slow LoS downward trend.

2). For instance, the combination of the slow uplift/subsidence trends detected in areas to the west of the PSDFS along the descending LoS in the Stages A, B, and D, with coeval apparent absence of PS motion along the ascending LoS (Fig. 4), may be explained by "real" PS motions occurring, with either east or west orientations, along a plane dipping at high angle with respect to the ascending LoS (Fig. 2B). As a result, the components of SAR-real displacement vector (i.e. displacement in a vertical, E-W oriented plane) are oriented towards up and east (Fig. 2B) during Stage A. Combining the two LoS-oriented motions during Stage B, the SAR-real displacement vector is oriented downwards with a westward component. The Stage C displacement inferred from PS motion along the two LoS corresponds to a vector oriented downwards (roughly vertical). The combination of the two LoS-oriented motions suggests a SAR-real displacement vector oriented downward (with a westward component) during Stage D.

The multi-temporal, spatial distribution of the vertical component of PS motion in the entire study region has been analysed by combining both the ascending and descending displacement components. In order to select homogeneous ranges in the displacement orientation, we have separately analysed the time spans corresponding to the stages A to D that have been distinguished by analysis of the descending PS time series (Fig. 4B).

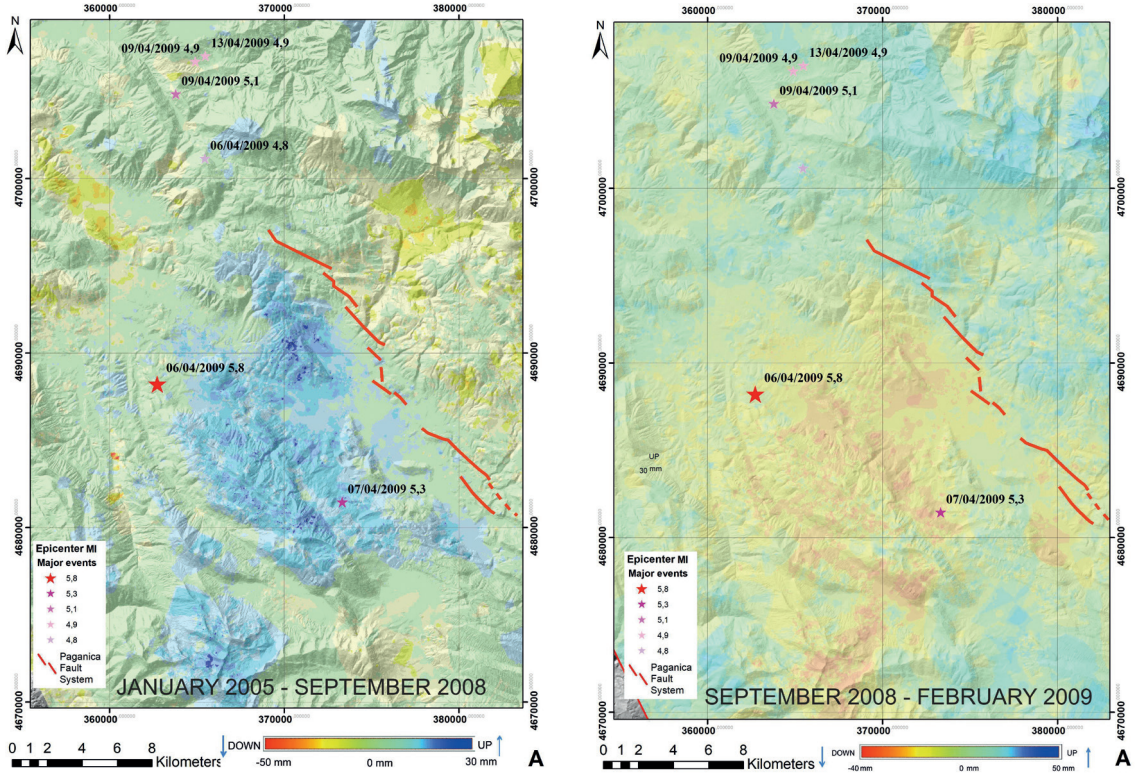

Fig. 5 - Pre-seismic deformation pattern [IDW (50×50 m^2 cell size) spatial interpolation] in the study region. A: cumulative vertical (z) ground deformation during Stage A (January 2005 - September 2008); mean uplift ca. 10 mm in the PSDFS hanging wall block; the footwall block is affected by slight subsidence. B: cumulative vertical (z) ground deformation during Stage B (September 2008 - February 2009); mean subsidence ca. 10 mm in the PSDFS hanging wall block; the footwall block shows a slight uplift.

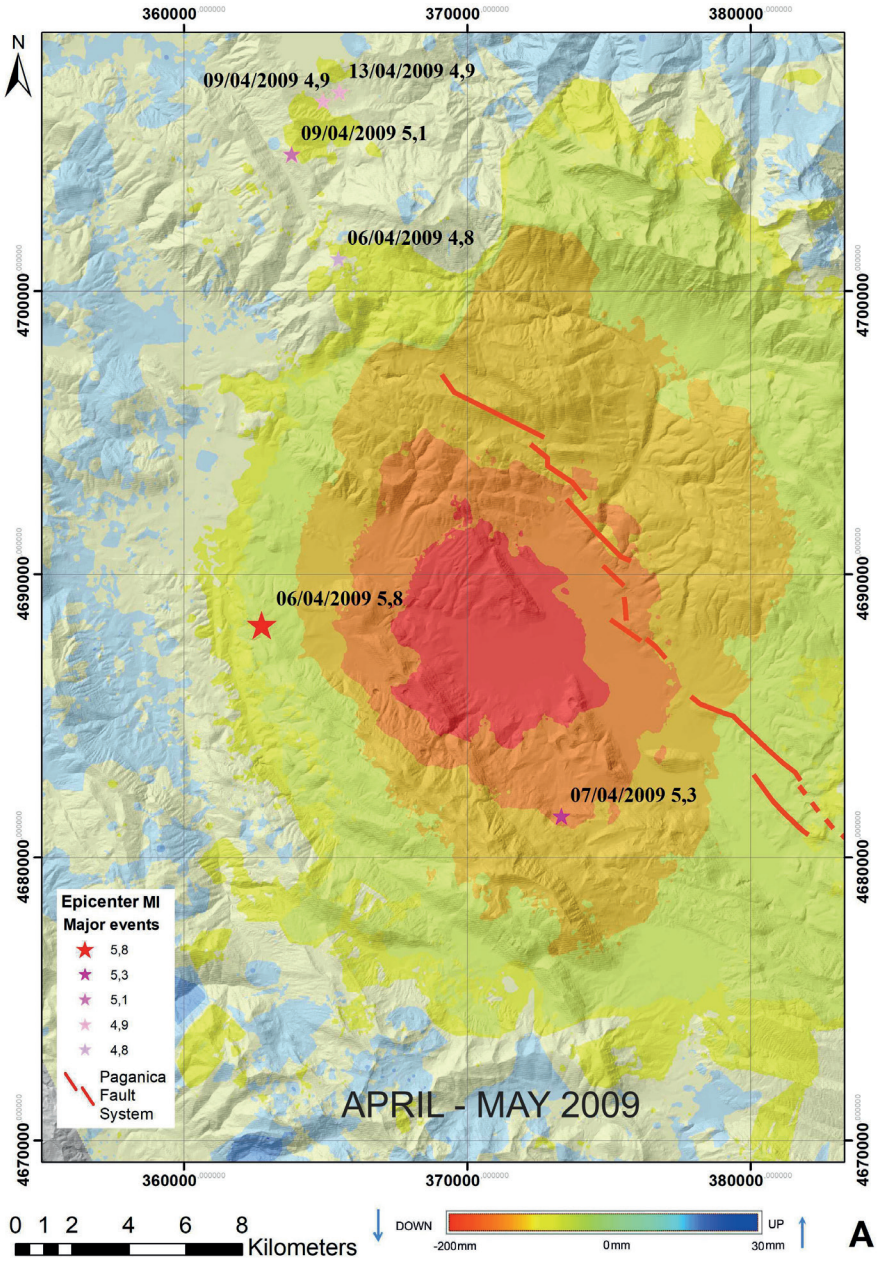

Fig. 6 - Co- to early post-seismic deformation pattern during STAGE C [IDW (50×50 m^2 cell size) spatial interpolation] in the study region. Total vertical ground deformation from February 2009 to May 2009; cumulative mean subsidence ca. 80 mm with maximum values located in the PSDFS hanging wall block.

The maps of Fig. 5 show the values of the vertical displacement cumulated during stages A (January 2005 - September 2008) and B (September 2008 - February 2009), respectively. The map of Fig. 5A shows that, during Stage A, a large area covering the 2009 main shock underwent uplift with mean values around 10 mm (the corresponding displacement along the descending LoS has a mean value of ~18±6 mm) and maximum values of ~ 25 mm. During Stage B (Fig. 5B), the same area that in Stage A had been uplifted underwent negative vertical displacement

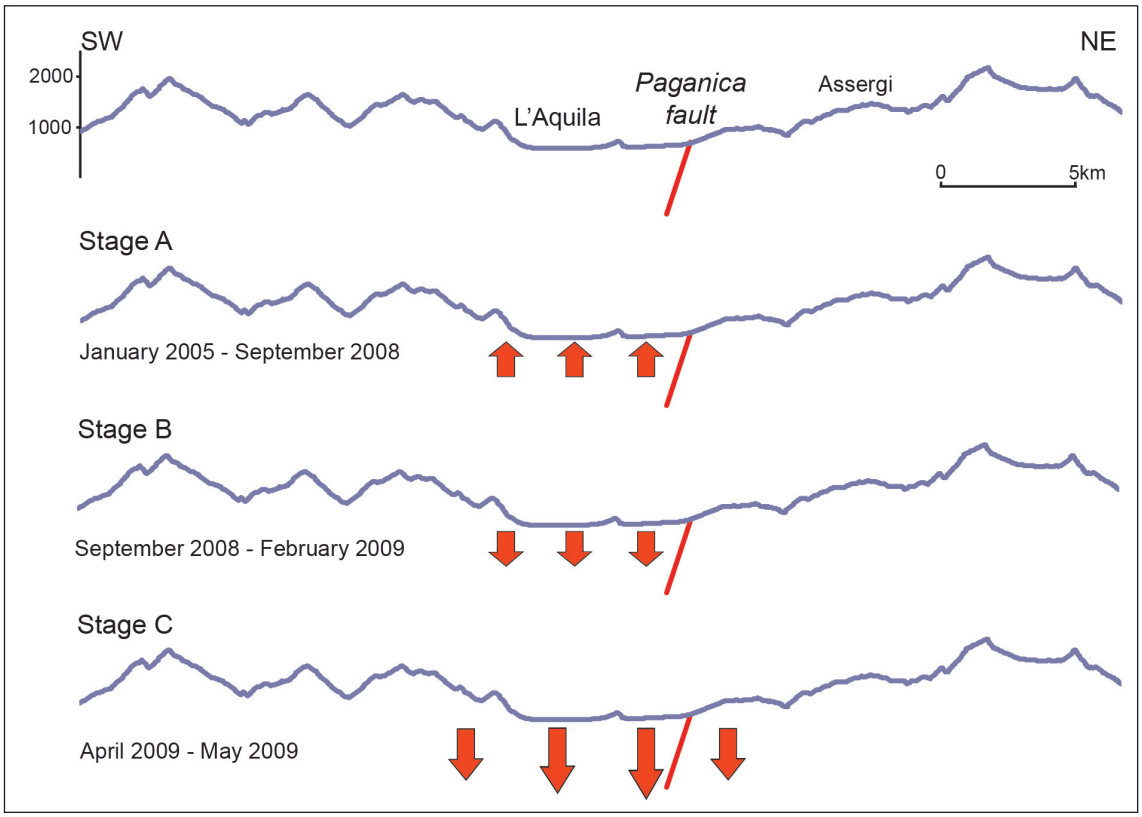

Fig. 7 - Topographic profiles, SW-NE oriented, constructed transversely to the Paganica segment of the PSDFS. The profiles synthesise cumulative pre-seismic vertical displacement patterns in the pre-seismic period (Stage A; from 2004 to September/October 2008), late pre-seismic period (Stage B; September/October 2008 to January/February 2009), and co- to early post-seismic period (Stage C; April to May 2009), respectively.

with mean values around 10 mm (the corresponding displacement along the descending LoS has a mean value of ~ -14±6 mm). The spatial distribution of the co- to early post-seismic displacement is shown in the map of Fig. 6, in which a sudden collapse with mean values of ~ 80 mm (and maximum values in the 180-200 mm range) is visible.

The profiles of Fig. 7 synthesise the time-space evolution of vertical motions along a transect cut across the study region. In the profiles, ground deformation is represented. The profiles of Fig. 7 show that the trace of the PSDFS falls between the block to the SW, which underwent uplift during Stage A and subsidence during Stage B, and the initially lowered and then uplifted block to the NE. A complex deformation pattern is highlighted by the bottom profile of Fig. 7, which shows that the area that collapsed during Stage C includes part of the elevations to the SW and NE of the central sector of the Aterno River valley.

5. Discussion and concluding remarks

The multi-temporal, spatial analysis of ground deformation that we have performed through analyses of PS-InSAR data sets, provides evidence for important features of the displacements

that accompanied the evolution of the 2009 seismic phenomenon occurring in the L'Aquila region during the pre- to post-seismic periods.

The analysed PS data sets bear a combination of time-variable motions, including apparent ground motion, which may be caused by atmospheric artefacts (e.g. Hanseen, 2001). Such an effect, which is very variable in time, may be considered responsible for irregular noisy patterns (Atzori *et al*., 2013), such as those characterising the time series from the ERS ascending orbit shown in Fig. 3B. Besides such irregular signals, short-period - seasonal - ground motions in the range of ~ ±10 mm, which are the main feature of the PS time series from the ERS descending and ascending orbits (Fig. 3) and of the pre- and post-seismic periods of the ascending ENVISAT PS time series (Fig. 4A), may be related to seasonal fluctuations in the piezometric head of the groundwater tables (Vilardo *et al*., 2009; Bozzano *et al*., 2015). Monthly-scale fluctuations also characterise the descending ENVISAT PS time series, though such a signal is subordinate, in terms of magnitude and temporal persistence, with respect to LoS oriented linear trends observed on the yearly scale time window (2003-2010; Fig. 4B).

Besides irregular and/or short period, spatially variable motions, the ERS PS time series show yearly scale sub-horizontal trends, and the combination of ascending/descending pairs has shown that no net displacement affected the analysed region in the 1992-2000 time span.

A more complex scenario has been reconstructed for the narrow time window covered by the ENVISAT PS data, and in particular for the pre-seismic period. Consistent with findings by Lanari *et al*. (2010), data acquired from the ENVISAT ascending orbit do not show clear pre-seismic (as well as "late" post-seismic) ground displacement trends. We interpret such evidence as an effect of the geometry of the SAR ascending orbit, which is basically unable to detect displacements within a plane at high angle with respect to the ascending LoS (section 4.2; Fig. 2B). On the other hand, the ascending data set has provided constraints on the orientations of the pre- to post-seismic displacement vectors. The PS time series from the descending orbit and the combined (ascending plus descending) data sets have allowed detecting temporally and spatially distributed pre-seismic motions. Within the pre-seismic ground deformation frame that we have reconstructed, the PSDFS marks the boundary between blocks that underwent vertical motions with opposite orientations (Fig. 5). In particular, uplift, followed by subsidence, affected a large area that covers the PSDFS hanging wall block. The "early" pre-seismic uplift, which produced mean vertical displacements in the order of 10 mm, started ~ 4-5 years before the April 2009 main shock, coeval with both slow subsidence of the region to the NE that includes the PSDFS footwall block (Figs. 5A and 7), and subsidence detected by Moro *et al*. (2017) in the Pizzoli and Petruro sub-basins of the middle Aterno valley, to the NW of the uplifted area (Figs. 1 and 5A).

At ~ 6-8 month prior to the April 2009 main shock, an up-down inversion of vertical displacement affecting the blocks separated by the PSDFS is recorded (Fig. 8). Vertical displacements summed up during such time span were in the same order of those recorded during the former (and longer) stage.

The co- to early post-seismic vertical displacement picture is consistent with that provided by former studies based on analyses of SAR data and GPS and/or levelling data (e.g. Atzori *et al*., 2009; Cirella *et al*., 2009; Walters *et al*., 2009; Cheloni *et al*., 2010). In addition, our spatial analysis indicates that the collapsed area extends to the NE beyond the PSDFS trace (Figs. 6 and 7), and allows detecting several steps in the displacement profile (Fig. 7), which may suggest the occurrence of possible co-seismic ruptures along the belts to the SW and NE of the area affected by maximum subsidence. The descending PS time series highlight post-seismic subsidence in the hanging wall

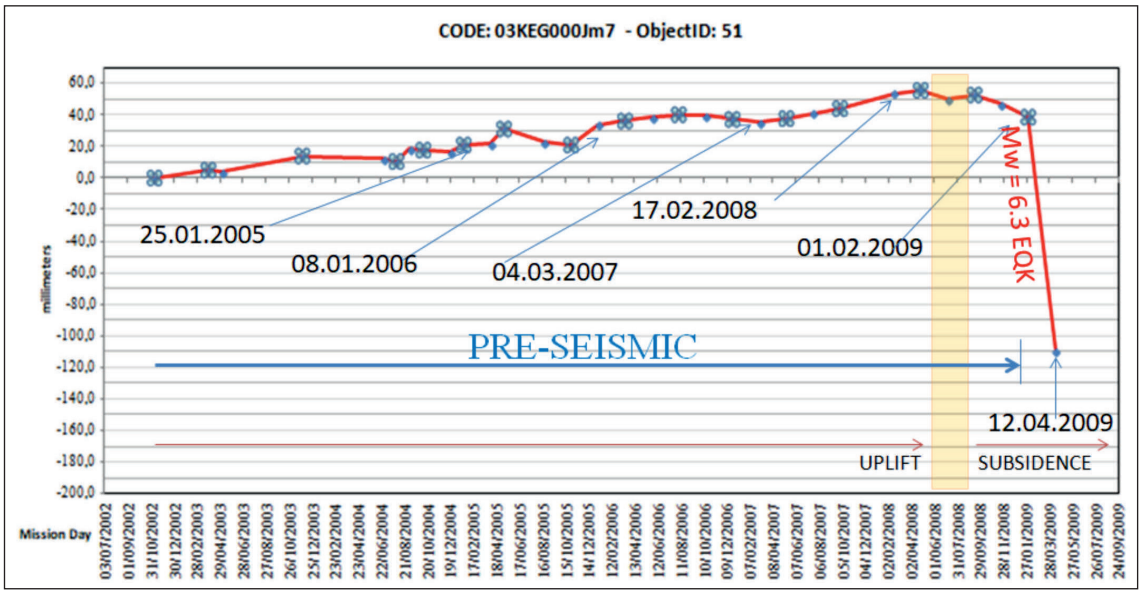

Fig. 8 - Time intervals of about one year in which the ENVISAT satellite detected the distance of a PS along the descending LoS (LoS uplift). From the end of 2008 (6-8 months prior to the main shock) and the first months of 2009, the yearly uplift trend changed to subsidence.

of the PSDFS continuing at least until June 2010, consistent with evidence both provided by D'Agostino *et al*. (2012) based on GPS and InSAR data, and detected by Galli *et al*. (2010) of a few cm increase of vertical offsets of several coseismic fractures in the first months after the main shock.

The geometrical combination of the ascending and descending PS-InSAR data indicates that the displacements are not entirely vertical, but are characterised by horizontal components oriented towards either east or west (section 4.2). Such evidence suggests that magnitude of "real" displacements, which in the co- to post-seismic period includes south/north-oriented components [as shown by GPS data: Cheloni *et al*. (2014)] that are undetectable by SAR data, is larger than that evaluated with this study.

The detection by remotely sensed data of the subdued pre-seismic ground displacements that we have identified rests on a thorough multi-temporal analysis of data by satellite image pairs. Indeed, the combined analysis of PS-InSAR data sets from both the ascending and descending orbits has been crucial to unravelling the pre-seismic behaviour of the study region.

The peculiar pre-seismic behaviour of the PSDFS hanging wall points to a relationship of the near-field surface motions with seismic phenomena. Such a relationship is also inferred from evidence that the region affected by rise followed by lowering lies in the area where the main shock and most of both foreshocks and aftershocks (Valoroso *et al*., 2013) are contained, and from the chronological correlation of the up/down inversion in the pre-seismic displacements with onset of the foreshocks [October 2008: Di Luccio *et al*. (2010)]. Worthy of note, the spatial scale of such a region (which encompasses both topographic highs and lows) is independent from surface geology features, suggesting a deep-seated causative mechanism for the observed motions, such as for instance volume changes connected to vertical/lateral fluids migration and fracturing processes at depth, with all phenomena having been documented in connection with

the 2009 earthquake in the study region (e.g. Di Luccio *et al*., 2010; Lucente *et al*., 2010; Moro *et al*., 2017).

We suggest that pre-seismic displacements, such as those characterising the hanging wall and footwall blocks of the PSDFS, may collectively represent a precursor signal of the 2009, M_W 6.3 earthquake. Our results point to the long-term (yearly scale) multitemporal InSAR data analysis as a crucial tool for detecting ground deformation in areas struck by recent earthquakes and for monitoring active structures.

Acknowledgements. We are grateful to Paolo Galli and Giuliana Rossi for their careful review and constructive criticism, which helped us improve the work. This work was presented at the 36° Convegno Nazionale Gruppo Nazionale di Geofisica della Terra Solida, Trieste, 14-16 November 2017.

REFERENCES

Achache J., Fruneau B., and Delacourt C.; 1995: *Applicability of SAR Interferometry for Monitoring of Landslides*. In: Proc. 2nd International Workshop, ERS Applications, Guyenne T.-D. (ed), London, England, ESA SP-383, 165 p.

Amoruso, A. and Crescentini L.; 2010: *Limits on earthquake nucleation and other pre-seismic phenomena from continuous strain in the near field of the 2009 L'Aquila earthquake*. Geophys. Res. Lett., **37**, L10307, doi:10.1029/2010GL043308.

Anzidei M., Boschi E., Cannelli V., Devoti R., Esposito A., Galvani A., Melini D., Pietrantonio G., Riguzzi F., Sepe V. and Serpelloni E.; 2009: *Coseismic deformation of the destructive April 6, 2009 L'Aquila earthquake (central Italy) from GPS data*. Geophys. Res. Lett., **36**, L17307, doi:10.1029/2009GL039145.

Atzori S., Hunstad I., Chini M., Salvi S., Tolomei C., Bignami C., Stramondo S., Trasatti E., Antonioli A. and Boschi E.; 2009: *Finite fault inversion of DInSAR coseismic displacement of the 2009 L'Aquila earthquake (central Italy)*. Geophys. Res. Lett., **36**, L15305, doi:10.1029/2009GL039293.

Atzori S., Chiarabba C., Devoti R., Bonano M. and Lanari R.; 2013: *Anomalous far-field geodetic signature related to the 2009 L'Aquila (central Italy) earthquake*. Terra Nova, **25**, 343-351, doi:10.1111/ter.12040.

Berardino P., Fornaro G., Lanari R. and Sansosti E.; 2002: *A new algorithm for surface deformation monitoring based on small baseline differential SAR interferograms*. IEEE Trans. Geosci. Rem. Sens., **40**, 2375-2383.

Boncio P., Pizzi A., Brozzetti F., Pomposo G., Lavecchia G., Di Naccio D. and Ferrarini F.; 2010: *Coseismic ground deformation of the 6 April 2009 L'Aquila earthquake (central Italy, Mw 6.3)*. Geophys. Res. Lett., **37**, L06308.

Bozzano F., Esposito C., Franchi S., Mazzanti P., Perissin D., Rocca A. and Romano E.; 2015: *Understanding the subsidence process of a quaternary plain by combining geological and hydrogeological modelling with satellite InSAR data: the Acque Albule Plain case study*. Remote Sens. Environ., **168**, 219-238.

Bürgmann R., Hilley G., Ferretti A. and Novali F.; 2006: *Resolving vertical tectonics in the San Francisco Bay Area from permanent scatterer InSAR and GPS analysis*. Geol., **34**, 221-224.

Carnec C., Massonnet D. and King C.; 1996: *Two examples of the use of SAR interferometry on displacement fields of small spatial extent*. Geophys. Res. Lett., **23**, 3579-3582.

Cheloni D., D'Agostino N., D'Anastasio E., Avallone A., Mantenuto S., Giuliani R., Mattone M., Calcaterra S., Gambino P., Dominici D., Radicioni F. and Fastellini G.; 2010: *Coseismic and initial post-seismic slip of the 2009 Mw 6.3 L'Aquila earthquake, Italy, from GPS measurements*. Geophys. J. Int., **181**, 1539-1546.

Cheloni D., Giuliani R., D'Anastasio E., Atzori S., Walters R.J., Bonci L., D'Agostino N., Mattone M., Calcaterra S., Gambino P., Deninno F., Maseroli R. and Stefanelli G.; 2014: *Coseismic and post-seismic slip of the 2009 L'Aquila (central Italy) Mw 6.3 earthquake and implications for seismic potential along the Campotosto Fault from joint inversion of high-precision levelling, InSAR and GPS data*. Tectonophys., **622**, 168-185.

Cheloni D., De Novellis V., Albano M., Antonioli A., Anzidei M., Atzori S., Avallone A., Bignami C., Bonano M., Calcaterra S., Castaldo R., Casu F., Cecere G., De Luca C., Devoti R., Di Bucci D., Esposito A., Galvani A., Gambino P., Giuliani R., Lanari R., Manunta M., Manzo M., Mattone M., Montuori A., Pepe A., Pepe S., Pezzo G., Pietrantonio G., Polcari M., Riguzzi F., Salvi S., Sepe V., Serpelloni E., Solaro G., Stramondo S., Tizzani P., Tolomei C., Trasatti E., Valerio E., Zinno I. and Doglioni C.; 2017: *Geodetic model of the 2016 central Italy earthquake sequence inferred from InSAR and GPS data*. Geophys. Res. Lett., **44**, 6778-6787, doi:10.1002/2017GL073580.

Chiarabba C., Amato A., Anselmi M., Baccheschi P., Bianchi I., Cattaneo M., Cecere G., Chiaraluce L., Ciaccio M.G., De Gori P., De Luca G., Di Bona M., Di Stefano R., Faenza L., Govoni A., Improta L., Lucente F.P., Marchetti A., Margheriti L., Mele F., Michelini A., Monachesi G., Moretti M., Pastori M., Piana Agostinetti N., Piccinini D., Roselli P., Seccia D. and Valoroso L.; 2009: *The 2009 L'Aquila (central Italy) Mw 6.3 earthquake: main shock and aftershocks*. Geophys. Res. Lett., **36**, L18308, doi:10.1029/2009GL039627.

Chiaraluce L., Valoroso L., Piccinini D., Di Stefano R. and De Gori P.; 2011: *The anatomy of the 2009 L'Aquila normal fault system (central Italy) imaged by high resolution foreshock and aftershock locations*. J. Geophys. Res.: Solid Earth, **116**, B12311, doi:10.1029/2011JB008352.

Cirella A., Piatanesi A., Cocco M., Tinti E., Scognamiglio L., Michelini A., Lomax A. and Boschi E.; 2009: *Rupture history of the 2009 L'Aquila (Italy) earthquake from non-linear joint inversion of strong motion and GPS data*. Geophys. Res. Lett., **36**, L19304, doi:10.1029/2009GL039795.

Corsini A., Farina P., Antonello G., Barbieri M., Casagli N., Coren F., Guerri L., Ronchetti F., Sterzai P. and Tarchi D.; 2006: *Space-borne and ground-based SAR interferometry as tools for landslide hazard management in civil protection*. Int. J. Remote Sens., **27**, 2351-2369.

Costantini M., Ferretti A., Minati F., Falco S., Trillo F., Colombo D., Novali F., Malvarosa F., Mammone F., Vecchioli F., Rucci A., Fumagalli A., Allievi J., Ciminelli M.G. and Costabile S.; 2017: *Analysis of surface deformations over the whole Italian territory by interferometric processing of ERS, Envisat and COSMO-SkyMed radar data*. Remote Sens. Environ., **202**, 250-275.

D'Agostino N., Cheloni D., Fornaro G., Giuliani R. and Reale D.; 2012: *Space-time distribution of afterslip following the 2009 L'Aquila earthquake*. J. Geophys. Res., **117**, B02402.

Di Luccio F., Ventura G., Di Giovambattista R., Piscini A. and Cinti F.R.; 2010: *Normal faults and thrusts reactivated by deep fluids: the 6 April 2009 Mw 6.3 L'Aquila earthquake, central Italy*. J. Geophys. Res., **115**, B06315, doi:10.1029/2009JB007190.

EMERGEO Working Group; 2010: *Evidence for surface rupture associated with the Mw 6.3 L'Aquila earthquake sequence of April 2009 (central Italy)*. Terra Nova, **22**, 43-51.

Falcucci E., Gori S., Peronace E., Fubelli G., Moro M., Saroli M., Giaccio B., Messina P., Naso G., Scardia G., Sposato A., Voltaggio M., Galli P. and Galadini F.; 2009: *The Paganica Fault and surface coseismic ruptures caused by the 6 April 2009 earthquake (L'Aquila, central Italy)*. Seismol. Res. Lett., **80**, 940-950.

Ferretti A., Prati C. and Rocca F.; 2000: *Nonlinear subsidence rate estimation using permanent scatterers in differential SAR interferometry*. IEEE Trans. Geosci. Remote Sens., **38**, 2202-2212.

Ferretti A., Prati C. and Rocca F.; 2001: *Permanent scatters in SAR interferometry*. IEEE Trans. Geosci. Remote Sens., **39**, 8-20.

Fruneau B., Achache J. and Delacourt C.; 1996: *Observation and modelling of the Saint-Étienne-de-Tinée landslide using SAR interferometry*. Tectonophys., **265**, 181-190.

Galli P., Camassi R., Azzaro R., Bernardini F., Castenetto S., Molin D., Peronace E., Rossi A., Vecchi M. and Tertulliani A.; 2009: *Il terremoto aquilano del 6 aprile 2009: rilievo macrosismico, effetti di superficie ed implicazioni sismotettoniche*. Il Quaternario, **22**, 235-246.

Galli P., Giaccio B. and Messina P.; 2010: *The 2009 central Italy earthquake seen through 0.5 Myr-long tectonic history of the L'Aquila Faults system*. Quat. Sci. Rev., **29**, 3768-3789.

Galli P., Giaccio B., Messina P. and Peronace E.; 2011: *Paleoseismology of the L'Aquila Faults (central Italy, 2009 Mw 6.3 earthquake). Clues on active fault linkage*. Geophys. J. Int., **187**, 1119-1134, doi:10.1111/j.1365-246X.2011.05233.x.

Hanseen R.F.; 2001: *Radar interferometry: data interpretation and error analysis*. Kluwer Academic Publishers, Dordrecht, the Netherlands, 308 pp.

Jordan T.H., Chen Y.T., Gasparini P., Madariaga R., Main I., Marzocchi W., Papadopoulos G., Sobolev G., Yamaoka K. and Zschau J.; 2011: *Operational earthquake forecasting; state of knowledge and guidelines for utilization*. Ann. Geophys., **54**, 315-391.

Kimura H. and Yamaguchi Y.; 2000: *Detection of landslide areas using satellite radar interferometry*. Photogram. Eng. Remote Sens., **66**, 337-344.

Lanari R., Casu F., Manzo M., Zeni G., Berardino P., Manunta M. and Pepe A.; 2007: *An overview of the small BAseline subset algorithm: a DInSAR technique for surface deformation analysis*. In: Wolf D. and Fernández J. (eds), Deformation and gravity change: indicators of isostasy, tectonics, volcanism, and climate change, Pageoph Topical Volumes, Birkhäuser Basel, Switzerland, pp. 637-661.

Lanari R., Berardino P., Bonano M., Casu F., Manconi A., Manunta M., Manzo M., Pepe A., Pepe S., Sansosti E., Solaro G., Tizzani P. and Zeni G.; 2010: *Surface displacements associated with the L'Aquila 2009 Mw 6.3 earthquake (central Italy): new evidence from SBAS-DInSAR time series analysis*. Geophys. Res. Lett., **37**, L20309.

Lavecchia G., Boncio P., Brozzetti F., de Nardis R., di Naccio D., Ferrarini F., Pizzi A. and Pomposo G.; 2009: *The April 2009 L'Aquila (central Italy) seismic sequence (Mw 6.3): a preliminary seismotectonic picture*. In: Guarnieri P. (ed), Recent Progress on Earthquake Geology, Nova Science Publishers Inc., Hauppauge, NY, USA, Chapter 1, 17 pp.

Lucente F.P., De Gori P., Margheriti L., Piccinini D., Di Bona M., Chiarabba C. and Piana Agostinetti N.; 2010: *Temporal variation of seismic velocity and anisotropy before the 2009 Mw 6.3 L'Aquila earthquake, Italy*. Geol., **38**, 1015-1018, doi:10.1130/G31463.1.

Lundgren P., Casu F., Manzo M., Pepe A., Berardino P., Sansosti E. and Lanari R.; 2004: *Gravity and magma induced spreading of Mount Etna Volcano revealed by satellite radar interferometry*. Geophys. Res. Lett., **31**, L04602.

Manzo M., Ricciardi G.P., Casua F., Ventura G., Zeni G., Borgström S., Berardino P., Del Gaudio C. and Lanari R.; 2006: *Surface deformation analysis in the Ischia Island (Italy) based on spaceborne radar interferometry*. J. Volcanol. Geother. Res., **151**, 399-416.

Massonnet D. and Rabaute T.; 1993: *Radar interferometry: limits and potential*. IEEE Trans. Geosci. Remote Sens., **31**, 455-464.

Meisina C., Zucca F., Fossati D., Ceriani M. and Allievi J.; 2006: *Ground deformation monitoring by using the permanent scatterers technique: the example of the Oltrepo Pavese (Lombardia, Italy)*. Eng. Geol., **88**, 240-259.

Moro M., Saroli M., Stramondo S., Bignami C., Albano M., Falcucci E., Gori S., Doglioni C., Polcari M., Tallini M., Macerola L., Novali F., Costantini M., Malvarosa F. and Wegmüller U.; 2017: *New insights into earthquake precursors from InSAR*. Sci. Rep., **7**, 12035, doi:10.1038/s41598-017-12058-3.

Papadopoulos G.A., Charalampakis M., Fokaefs A. and Minadakis G.; 2010: *Strong foreshock signal preceding the L'Aquila (Italy) earthquake (Mw 6.3) of 6 April 2009*. Nat. Hazards Earth Syst. Sci., **10**, 19-24.

Papanikolaou I.D., Foumelis M., Parcharidis I., Lekkas E.L. and Fountoulis I.G.; 2010: *Deformation pattern of the 6 and 7 April 2009, Mw = 6.3 and Mw = 5.6 earthquakes in L'Aquila (central Italy) revealed by ground and space based observations*. Nat. Hazards Earth Syst. Sci., **10**, 73-87.

Pondrelli S., Salimbeni S., Morelli A., Ekström G., Olivieri M. and Boschi E.; 2010: *Seismic moment tensors of the April 2009, L'Aquila (central Italy), earthquake sequence*. Geophys. J. Int., **180**, 238-242.

Prati C., Ferretti A. and Perissin D.; 2010: *Recent advances on surface ground deformation measurement by means of repeated space-borne SAR observations*. J. Geodyn., **49**, 161-170.

Santo A., Ascione A., Di Crescenzo G., Miccadei E., Piacentini T. and Valente E.; 2014: *Tectonic-geomorphological map of the middle Aterno River valley (Abruzzo, central Italy)*. J. Maps, **10**, 365-378.

Scognamiglio L., Tinti E., Michelini A., Dreger D.S., Cirella A., Cocco M., Mazza S. and Piatanesi A.; 2010: *Fast determination of moment tensors and rupture history: what has been learned from the 6 April 2009 L'Aquila earthquake sequence*. Seismol. Res. Lett., **81**, 892-906, doi:10.1785/gssrl.81.6.892.

Stramondo S., Tesauro M., Briole P., Sansosti E., Salvi S., Lanari R., Anzidei M., Baldi P., Fornaro G., Avallone A., Buongiorno M.F., Franceschetti G. and Boschi E.; 1999: *The September 26, 1997 Colfiorito, Italy, earthquakes: modeled coseismic surface displacement from SAR interferometry and GPS*. Geophys. Res. Lett., **26**, 883-886.

Tizzani P., Berardino P., Casu F., Euillades P., Manzo M., Ricciardi G.P., Zeni G. and Lanari R.; 2007: *Surface deformation of Long Valley caldera and Mono Basin, California, investigated with the SBAS - InSAR approach*. Remote Sens. Environ., **108**, 277-289.

Tofani V., Segoni S., Agostini A., Catani F. and Casagli N.; 2013: *Technical note: use of remote sensing for landslide studies in Europe*. Nat. Hazards Earth Syst. Sci., **13**, 299-309.

Valoroso L., Chiaraluce L., Piccinini D., Di Stefano R., Schaff D. and Waldhauser F.; 2013: *Radiography of a normal fault system by 64,000 high-precision earthquake locations: the 2009 L'Aquila (central Italy) case study*. J. Geophys. Res.: Solid Earth, **118**, 1156-1176, doi:10.1002/jgrb.50130.

Vilardo G., Ventura G., Terranova C., Matano F. and Nardò S.; 2009: *Ground deformation due to tectonic, hydrothermal, gravity, hydrogeological, and anthropic processes in the Campania Region (southern Italy) from permanent scatterers synthetic aperture radar interferometry*. Remote Sens. Environ., **113**, 197-212.

Walters R.J., Elliott J.R., D'Agostino N., England P.C., Hunstad I., Jackson J.A., Parsons B., Phillips R.J. and Roberts G.; 2009: *The 2009 L'Aquila earthquake (central Italy): a source mechanism and implications for seismic hazard*. Geophys. Res. Lett., **36**, L17312, doi:10.1029/2009GL039337.

Corresponding author: Sergio Nardò
DISTAR, Dip. di Scienze della Terra, dell'Ambiente e delle Risorse
Complesso di Monte Sant'Angelo (Edificio L)
Via Cinthia, 21 - 80126 NAPOLI
Phone: +39 3337324107; e-mail: sergio.nardo@unina.it, s.nardo@arpacampania.it